

## Computer Methods in Biomechanics and Biomedical Engineering

Publication details, including instructions for authors and subscription information:

<http://www.tandfonline.com/loi/gcmb20>

### Effect of exercise on blood flow through the aortic valve: a combined clinical and numerical study

Hamidreza Ghasemi Bahraseman<sup>a</sup>, Kamran Hassani<sup>a</sup>, Mahdi Navidbakhsh<sup>b</sup>, Daniel M. Espino<sup>c</sup>, Zahra Alizadeh Sani<sup>d</sup> & Nasser Fatouraei<sup>e</sup>

<sup>a</sup> Department of Biomechanics, Science and Research Branch, Islamic Azad University, Tehran, Iran

<sup>b</sup> Department of Mechanical Engineering, Iran University of Science and Technology, Tehran, Iran

<sup>c</sup> School of Mechanical Engineering, University of Birmingham, Birmingham, England, UK

<sup>d</sup> Department of Cardiovascular Imaging, Shaheed Rajaei Cardiovascular, Medical and Research Center, Tehran University of Medical Science, Tehran, Iran

<sup>e</sup> Department of Biomedical Engineering, Amirkabir University, Tehran, Iran

Version of record first published: 26 Mar 2013.

To cite this article: Hamidreza Ghasemi Bahraseman, Kamran Hassani, Mahdi Navidbakhsh, Daniel M. Espino, Zahra Alizadeh Sani & Nasser Fatouraei (2013): Effect of exercise on blood flow through the aortic valve: a combined clinical and numerical study, *Computer Methods in Biomechanics and Biomedical Engineering*, DOI:10.1080/10255842.2013.771179

To link to this article: <http://dx.doi.org/10.1080/10255842.2013.771179>

PLEASE SCROLL DOWN FOR ARTICLE

Full terms and conditions of use: <http://www.tandfonline.com/page/terms-and-conditions>

This article may be used for research, teaching, and private study purposes. Any substantial or systematic reproduction, redistribution, reselling, loan, sub-licensing, systematic supply, or distribution in any form to anyone is expressly forbidden.

The publisher does not give any warranty express or implied or make any representation that the contents will be complete or accurate or up to date. The accuracy of any instructions, formulae, and drug doses should be independently verified with primary sources. The publisher shall not be liable for any loss, actions, claims, proceedings, demand, or costs or damages whatsoever or howsoever caused arising directly or indirectly in connection with or arising out of the use of this material.

## Effect of exercise on blood flow through the aortic valve: a combined clinical and numerical study

Hamidreza Ghasemi Bahraseman<sup>a\*</sup>, Kamran Hassani<sup>a</sup>, Mahdi Navidbakhsh<sup>b</sup>, Daniel M. Espino<sup>c</sup>, Zahra Alizadeh Sani<sup>d</sup> and Nasser Fatourae<sup>e</sup>

<sup>a</sup>Department of Biomechanics, Science and Research Branch, Islamic Azad University, Tehran, Iran; <sup>b</sup>Department of Mechanical Engineering, Iran University of Science and Technology, Tehran, Iran; <sup>c</sup>School of Mechanical Engineering, University of Birmingham, Birmingham, England, UK; <sup>d</sup>Department of Cardiovascular Imaging, Shaheed Rajaei Cardiovascular, Medical and Research Center, Tehran University of Medical Science, Tehran, Iran; <sup>e</sup>Department of Biomedical Engineering, Amirkabir University, Tehran, Iran

(Received 18 April 2012; final version received 25 January 2013)

The aim of this study was to measure the cardiac output and stroke volume for a healthy subject by coupling an echocardiogram Doppler (echo-Doppler) method with a fluid–structure interaction (FSI) simulation at rest and during exercise. Blood flow through aortic valve was measured by Doppler flow echocardiography. Aortic valve geometry was calculated by echocardiographic imaging. An FSI simulation was performed, using an arbitrary Lagrangian–Eulerian mesh. Boundary conditions were defined by pressure loads on ventricular and aortic sides. Pressure loads applied brachial pressures with (stage 1) and without (stage 2) differences between brachial, central and left ventricular pressures. FSI results for cardiac output were 15.4% lower than Doppler results for stage 1 ( $r = 0.999$ ). This difference increased to 22.3% for stage 2. FSI results for stroke volume were undervalued by 15.3% when compared to Doppler results at stage 1 and 26.2% at stage 2 ( $r = 0.94$ ). The predicted mean backflow of blood was 4.6%. Our results show that numerical methods can be combined with clinical measurements to provide good estimates of patient-specific cardiac output and stroke volume at different heart rates.

**Keywords:** cardiac output; echo-Doppler flow; fluid–structure interaction; stroke volume

### 1. Introduction

Despite progress in prevention, diagnosis and treatment of cardiac disease, it is still the main cause of death in industrialised nations (Murphy and Xu 2012). Measurement of cardiac output is a key factor in detecting the development of cardiovascular diseases and making relevant clinical decisions (Criner et al. 2010). For example, heart failure could be explained as failure of the heart to maintain a cardiac output that supplies the metabolic demands of the body (Smith and Yeung 2010). Therefore, monitoring cardiac function during blood pumping and measuring stroke volume are important for diagnosing such diseases. Currently, invasive methods are typically used to measure cardiac output and/or stroke volume. However, such procedures are difficult, expensive and can have risks associated with them (Lavdaniti 2008). Computational methods, however, have the potential to determine the cardiac output and the stroke volume, thus removing the need for invasive procedures.

Several clinical methods exist for measuring the cardiac output including angiography, catheterisation, magnetic resonance imaging and ultrasound. Some of these methods are invasive, while others require the availability of large scale and expensive equipment (Engoren and Barbee 2005; Hofer et al. 2007; Lavdaniti 2008). Clinically, it has been shown that cardiac output

and stroke volume can be determined from the consumed breath-by-breath oxygen and released carbon monoxide while exercising on a bicycle (Knobloch et al. 2007a). That study used non-invasive ultrasound-Doppler imaging on healthy adult athletes. The measurements were taken from a rest position and continued by increasing the patient's velocity on a bicycle. They found correlations between cardiac output, cardiac index, heart rate, stroke volume and consumed  $O_2$ . Sugawara et al. (2003) tried to calculate the cardiac output using a model-flow method. They compared their results to the data extracted by echocardiogram Doppler (echo-Doppler) and claimed that the model-flow technique gave more accurate cardiac output measurements than echo-Doppler. Knobloch et al. (2007b) compared two clinical techniques, ultrasound cardiac output monitoring and Stringer's formula for non-invasive haemodynamics in exercise testing (Stringer et al. 1997), which were used to measure the cardiac output. In a study by Christie et al. (1987), three different methods were used to estimate and compare cardiac the output. Maroni et al. (1998) instead used a first-pass radionuclide ventriculographic method to calculate the cardiac output and even diagnosed myocardial dysfunction. However, a non-invasive and inexpensive but relatively harmless method to determine the cardiac output is currently not available.

\*Corresponding author. Email: hamid\_ghasemi57@yahoo.com

Computational methods have the potential to predict the cardiac output, provided the correct boundary conditions are applied. In particular, simultaneous fluid–structure interaction (FSI) simulations are well suited to heart valve modelling. This is because opening and closure of the aortic valve is caused by the flow of blood (Caro et al. 1978) and altered by flow patterns (Bellhouse 1972). Iterative approaches can be used, but instabilities may arise (Peskin 1972, 1977). As the deformation of the valve alters the flow patterns, a simultaneous approach is ideal. FSI simulations determine the reaction force that a fluid exerts on the structure with which it shares a boundary (Dowell & Hall 2001; Van de Vosse et al. 2003; Wall et al. 2006). The fluid velocity is constrained to be equivalent to the structural time-dependent deformation; this ensures a two-way, and simultaneous, coupling (Dowell and Hall 2001; Van de Vosse et al. 2003; Wall et al. 2006). This method requires the use of an arbitrary Lagrange–Euler (ALE) mesh to analyse both structural deformation (by finite element analysis) and computational fluid dynamics (Donea et al. 1982; Formaggia and Nobile 1999).

Recently, FSI has been used to investigate biological (Al-Atabi et al. 2010; Espino et al. 2012a, 2012b) and mechanical (Stijnen et al. 2004; Xia et al. 2005) heart valves. The aortic valve, for example, has been simulated in two (De Hart et al. 2000) and three dimensions (De Hart et al. 2003a), and its leaflets have been simulated as fibre-reinforced composites (De Hart et al. 2003b). Such models demonstrate the feasibility to develop complicated aortic valve models. However, so far, they have not been combined with non-invasive clinical measurements to predict a patient's cardiac output. Changes to such predictions due to heart rate (e.g. due to exercise) have not been analysed either. Heart rate is an important parameter to consider because it can cause large differences in the cardiac output.

The aim of this study, therefore, was to calculate the cardiac output and the stroke volume during exercise using a two-dimensional (2D) FSI model of the aortic valve. The boundary conditions applied were based on the calculation of brachial pressures and accounted for differences in brachial, central and left ventricular pressures. The model operated as a natural aortic valve: an increasing systolic pressure caused valve opening and blood flow was ejected through the aortic artery. At the end of systole, as ventricular systolic pressure decreased, the aortic valve came to closure. Therefore, by combining non-invasive pressure measurements with an FSI simulation, it was possible to calculate peak velocity, mean velocity, velocity–time integration, cardiac output and stroke volume. These predictions were specific to the volunteer because the 2D model geometry and boundary conditions were determined from measurements on the volunteer. In a clinical setting, material properties were not available; therefore, these were taken from the literature. Model

validation was performed by comparing results to measurements from echocardiography (ECG).

## 2. Methods

### 2.1 Design of experiment

A healthy male, aged 33 years, participated in this study with his haemodynamic data recorded during rest and exercise. Such data have been compared to FSI simulation results. Informed consent was obtained for the participant according to protocols approved by the Department of Cardiovascular Imaging (Shaheed Rajaei Cardiovascular, Medical and Research Center, Tehran, Iran). Following physical examination, the volunteer was found to have normal cardiovascular performance, as determined from maximal bicycle exercise tests and Doppler ECG.

Exercise consisted of the volunteer pedalling on a bicycle, with the required images of blood flow through the aortic valve obtained from the heart's five-chamber view in the apex region using B-mode. The brachial pressure was recorded from subject's left arm. Exercise regimes consisted of the subject raising his heart rate to approximately 180 bpm by maximal bicycle exercise tests.

Section 2.2 describes the cardiovascular measurements and their use to calculate relevant haemodynamic parameters applied to define the geometry and boundary conditions of the model. The FSI model simulated is described in Section 2.3. Note that the FSI model has, therefore, been used to determine the flow through the aortic valve at a range of heart rates.

### 2.2 Cardiovascular measurements

#### 2.2.1 Echocardiography

A commercially available ultrasonograph (Maylab, 60, BIOSOUND ESAOTE Inc., CA, USA) was used for ECG examinations. A 4 MHz phased-array probe was located at the apex to observe the heart's five-chamber view in order to record the blood flow through aortic valve. The aortic valve geometry was obtained by placing a transducer at the position of the heart's three-chamber view. Blood flow was estimated by echo-Doppler flow at different heart rate stages from rest to maximal bicycle exercise test. The subject fixed his back to the bicycle chair to aid high quality images by ECG. Echo-Doppler images were stored digitally and analysed at a later stage using Maylab-desk analyser (Maylab, BIOSOUND ESAOTE Inc., USA). Only high-quality images were accepted for subsequent use.

#### 2.2.2 Peak ventricular systolic pressure and minimum central diastolic aortic pressure

Systolic and diastolic pressures of the brachial artery were measured and related to heart rate changes at rest and

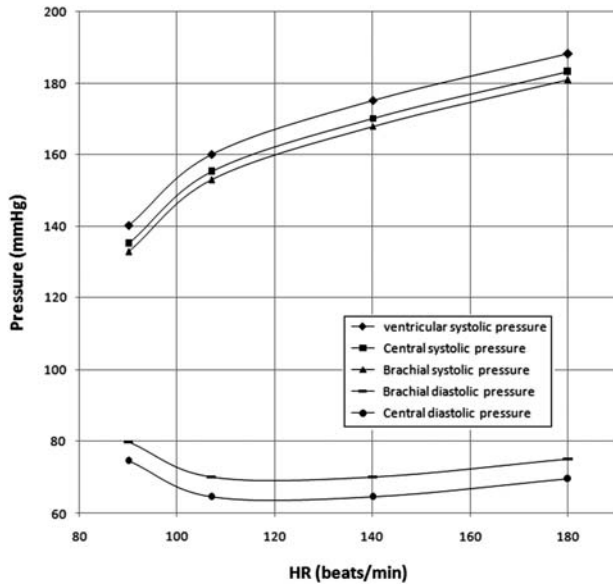


Figure 1. Interpolated curves for brachial, central and ventricular pressures.

exercise (Figure 1). Equations (1) and (2) were used to determine the central pressure from brachial pressure measurements. This relationship was previously determined by comparing brachial pressure (acquired by Oscillometry) to the central pressure acquired using an invasive method (Park et al. 2011).

$$\text{Central systolic pressure} \approx \text{Brachial systolic pressure} + 2.25, \quad (1)$$

$$\begin{aligned} \text{Central diastolic pressure} \\ \approx \text{Brachial diastolic pressure} - 5.45, \end{aligned} \quad (2)$$

where all pressures were measured in mmHg.

We intended to calculate left ventricular systolic pressure and central systolic pressure. Previously, a pressure difference of around 5 mmHg was found between peak left ventricular systolic pressure and central systolic pressure using catheterisation (Laske et al. 1996). The ventricular, brachial, and central pressures measured are presented in Figure 1.

### 2.2.3 Ejection time

The ejection time was derived from Doppler-flow imaging under B-mode. Maylab-desk software was used to calculate the ejection time with respect to the Doppler-imaging baseline and the related ECG simultaneously. This was done by tracing the Doppler flow with a more regular border and a larger area. Note that the ejection time is an important factor for plotting left ventricular systolic pressure.

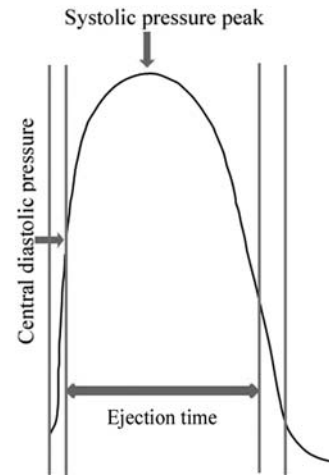


Figure 2. Tracings of the left ventricular systolic pressure waveform.

### 2.2.4 Time-dependent left ventricular pressure

Figure 2 shows the general waveform of left ventricle pressure versus ejection time (Guyton and Hall 1996). This waveform enabled us to derive left ventricular pressure waveform versus ejection time for each heart rate, including ejection time, left ventricular systolic pressure peak and central diastolic pressure. To do this, a scanned plot of the left ventricular pressure waveform versus ejection time was analysed using GetData Graph Digitizer (v 2.22). This software obtains original (pressure, time) data from the scanned plot and provides values for maximum/minimum ejection time and maximum pressure at the systolic pressure peak. The minimum central diastolic pressure at the start of diastole was also determined this way (Figure 2). These measurements provided the inflow boundary condition for the FSI model (Section 2.3.3).

## 2.3 Fluid–structure interaction simulation

### 2.3.1 Geometry

The intention was to measure the cardiac output at the cross-section of the aortic valve annulus. Therefore, aortic valve geometry was obtained with respect to the T-wave of ECG (maximum opening area). Diameters of the aortic valve annulus and the sinus valsalva were measured at the peak T-wave time using a resting para-sternal long-axis view. All required geometrical data are provided in Table 1. Using these data, a 2D model of the aortic root and chamber of aortic sinus valsalva was created (Figure 3) using Solidworks (Solidworks v2011, Dassault Systèmes SolidWorks Corp, France). The thickness of heart valve leaflets is not uniform (Clark and Finke 1974). In our model, however, we assumed the leaflets to have a uniform thickness (0.6 mm).

Table 1. Geometric data of the aortic valve.

Maximum diameter of normal aortic root (mm)	Ventricular side diameter (mm)	Aortic side diameter (mm)	Ascending aorta diameter after sinotubular junction (mm)	Leaflet's length (mm)	Valve's height (mm)
33.3	22.2	23	23.5	16.6	20.36

### 2.3.2 Material properties

The two leaflets were considered to be isotropic, homogeneous and have a linear stress–strain relationship. Blood was assumed to be an incompressible and Newtonian fluid. This is a valid assumption under large-scale flow, as it occurs through the left ventricle out towards the aorta (Caro et al. 1978). All material properties are provided in Table 2 and were obtained from the literature (Govindarajan et al. 2010; Koch et al. 2010).

### 2.3.3 Boundary conditions

For fluid boundaries (Figure 1), pressure was applied at the inflow boundary of the aortic root at the left ventricular side. The applied left ventricular pressures, for different

heart rates, are shown in Figure 4. Note that the peak pressure increased with heart rate, but the peak time of each curve decreased with increasing heart rate.

The condition of central diastolic pressure, which was heart rate dependent (Figure 1), was applied at the outflow boundary of the aortic heart valve (Figure 3). The walls of the aorta were set as no-slip and rigid boundaries (i.e. 0 m/s for the non-moving aortic walls). The flow condition at the shared boundaries of the valve leaflets in contact with the fluid domain was set to have a velocity equivalent to the velocity of the moving structure; i.e. the valve leaflet according to Equation (3).

$$u = \frac{\partial x}{\partial t}, \quad v = \frac{\partial y}{\partial t}, \quad (3)$$

where  $u$  and  $v$  refer to  $X$ - and  $Y$ -axis velocities, respectively, and  $\partial x/\partial t$  and  $\partial y/\partial t$  refer to the time-dependent displacement along the  $X$ -axis and  $Y$ -axis, respectively. Note that the  $Y$ -axis and  $X$ -axis define two orthogonal axes of a Cartesian coordinate system, where the former is parallel to the inflow and outflow boundaries of the aorta, while the latter is perpendicular to them (Figure 3).

For structural boundaries, leaflets were restricted from moving at their aortic wall attachment (Figure 3). Forces were induced by fluid dynamics, but a virtual spring constraint was applied to limit deflection (see Section 2.3.4). The force on the leaflet boundaries was induced by fluid flow and led to valve deflection (see Section 2.3.5).

### 2.3.4 Virtual spring constraints

The natural aortic valve has bowl-shaped leaflets that prevent the valve from opening evenly under high pressure during exercise (Stouffer 2008). We used a virtual spring with the equation:

$$f_s = -K \cdot (d - d_0) \quad (4)$$

Table 2. Mechanical properties.

Viscosity (Pa s)	Density (kg/m <sup>3</sup> )	Young's modulus (N/m <sup>2</sup> )	Poisson's ratio
$3.5 \times 10^{-3}$	1056	$6.885 \times 10^6$	0.4999

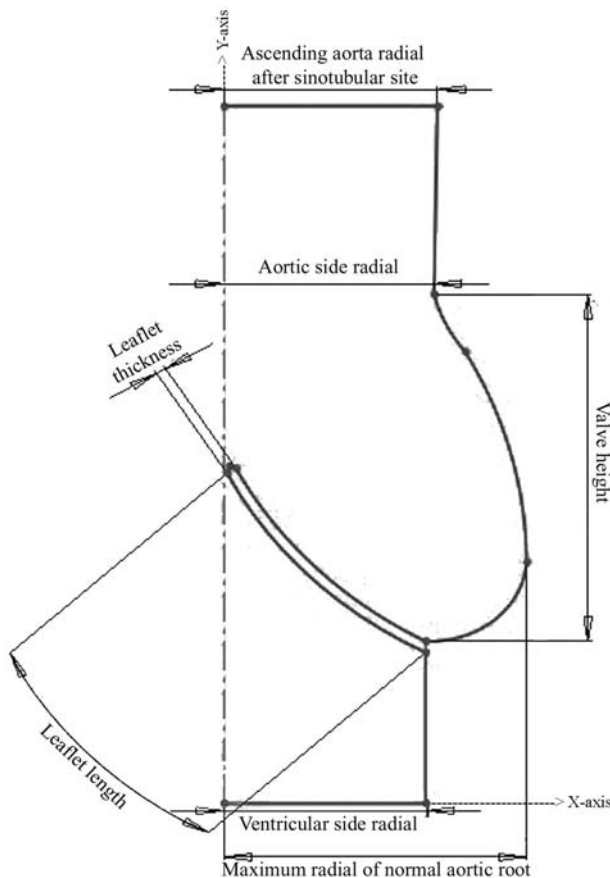


Figure 3. Aortic valve model. Note that dimensions are provided in Table 1.



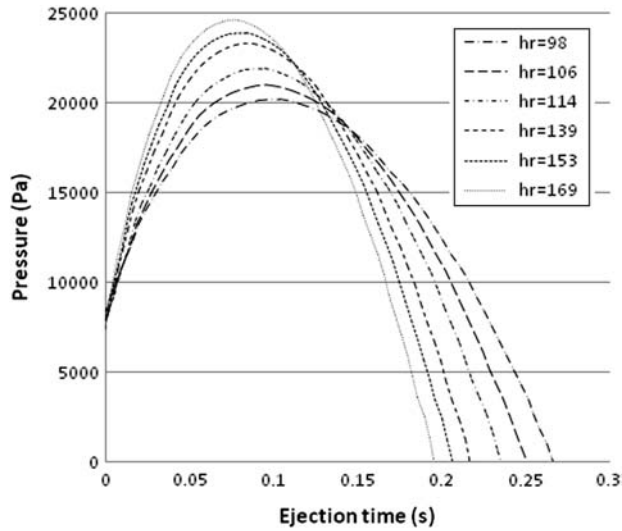


Figure 4. Pressure wave forms of the left ventricle during ejection for different heart rates.

to prevent excessive opening in our 2D model (Comsol 2011), where  $f_s$  is the force/unit area,  $d$  is the displacement and  $K$  is the diagonal stiffness matrix that was given a high value (approximately  $10^9$ ) to prevent excessive opening due to pressure load at the whole of simulation.  $d_o$  is an optional pre-deformation, assigned a value of zero because spring foundations act and connect to leaflets at the maximum leaflet tip distance, and at this time, pre-deformation equals zero for linked springs. Leaflet tip distance was estimated at full opening of the aortic valve by echo-Doppler imaging at rest. It was equal to 15.23 mm and held constant for all modelling stages at different heart rates.

### 2.3.5 Fluid–structure interaction

Simultaneous fluid and structure solution and their interaction require constraints that enforce such coupling. A velocity constraint (Equation (3)) coupled fluid flow to structural deformation. Equal and opposite reaction forces produced by the fluid applied loads to the structure. This ensured a two-way coupling (i.e. simultaneous interaction). The fluid forces are equivalent to Lagrange multipliers determined using a (non-ideal) weak formu-

lation of fluid dynamics. This led to the loading conditions expressed by Equation (5). Fluid dynamics were solved using the continuity and incompressible Navier–Stokes equations, assuming Newtonian and laminar flow, using a full stress tensor. Further detail on these techniques is provided elsewhere (Espino et al. 2012b).

$$(\boldsymbol{\sigma} \cdot \mathbf{n})_{\text{Fluid}} = (\boldsymbol{\sigma} \cdot \mathbf{n})_{\text{Solid}}, \quad (5)$$

where  $\boldsymbol{\sigma}$  is the stress tensor and  $\mathbf{n}$  is the normal vector to the FSI boundary (Comsol 2011).

A moving ALE mesh was used, which enabled a Lagrangian framework for the solid domain and an Eulerian framework for the fluid domain. The moving mesh enabled the deformation of the fluid mesh to be tracked. All other boundaries had a fixed mesh. No re-meshing was used, but Winslow smoothing was applied to improve the resultant mesh (Winslow 1966). The deformation of this mesh relative to the initial shape of the domain was also computed using hyper-elastic smoothing. 2D triangular planar strain elements were used to define the mesh. Mesh convergence was assessed in terms of stroke volume and cardiac output predictions (Table 3). Predictions were stable with 7001 elements (Figures 5 and 6). The number of elements was increased using predefined mesh sizes, which ranged from extremely coarse (1400 elements) to extra fine (19,865 elements) for our model.

FSI simulations modelled two different scenarios (termed stages). A stage with (stage 1) and without (stage 2) the valvular–arterial pressure differences between the aortic root at the left ventricle and the brachial artery was modelled. The results from these two stages demonstrated the effect of pressure drops in the predicted results (see Section 3.1).

### 2.3.6 Analysis

The finite element analysis package Comsol Multi-physics (v4.2) was used to solve the FSI model under time-dependent conditions. The structural mechanics package was used to analyse the leaflets. This enabled the use of a large deformation setting allowing determination of Green strains and Cauchy stresses as reported previously (Espino et al. 2012c).

Table 3. Investigation of mesh independency on predicted stroke volume and cardiac output, while considering valvular-arterial pressure differences, for a heart rate of 98 bpm.

Number of elements	1400 (Extremely coarse)	1944 (Extra coarse)	2194 (Coarser)	2648 (Coarse)	3669 (Normal)	5301 (Fine)	7001 (Finer)	19,865 (Extra fine)
Stroke volume (ml/beat)	94.9	95.2	96.7	96.1	99.1	100.7	100.9	100.9
Cardiac output (ml/min)	9300	9329	9476	9417	9711	9868	9888	9891
Solution time (s)	577	610	633	659	706	782	897	15,807

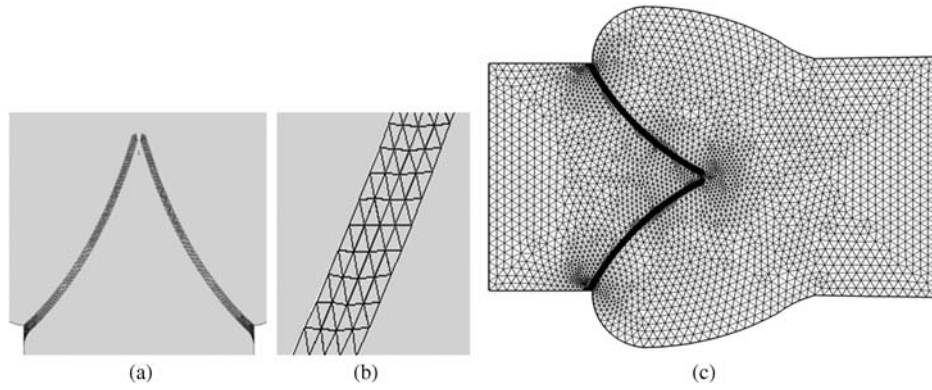


Figure 5. Mesh for the (a) valve cusps and (b) elements on a cusp of the solid domain mesh generation, (c) the fluid domain mesh generation.

A direct multifrontal massively parallel sparse direct solver (Comsol 2011) was used for the time-dependent simulation. Transition from one time step to the next

occurred once the estimated model error was below a set tolerance. A Newtonian iteration was used as discussed previously (Espino et al. 2012c).

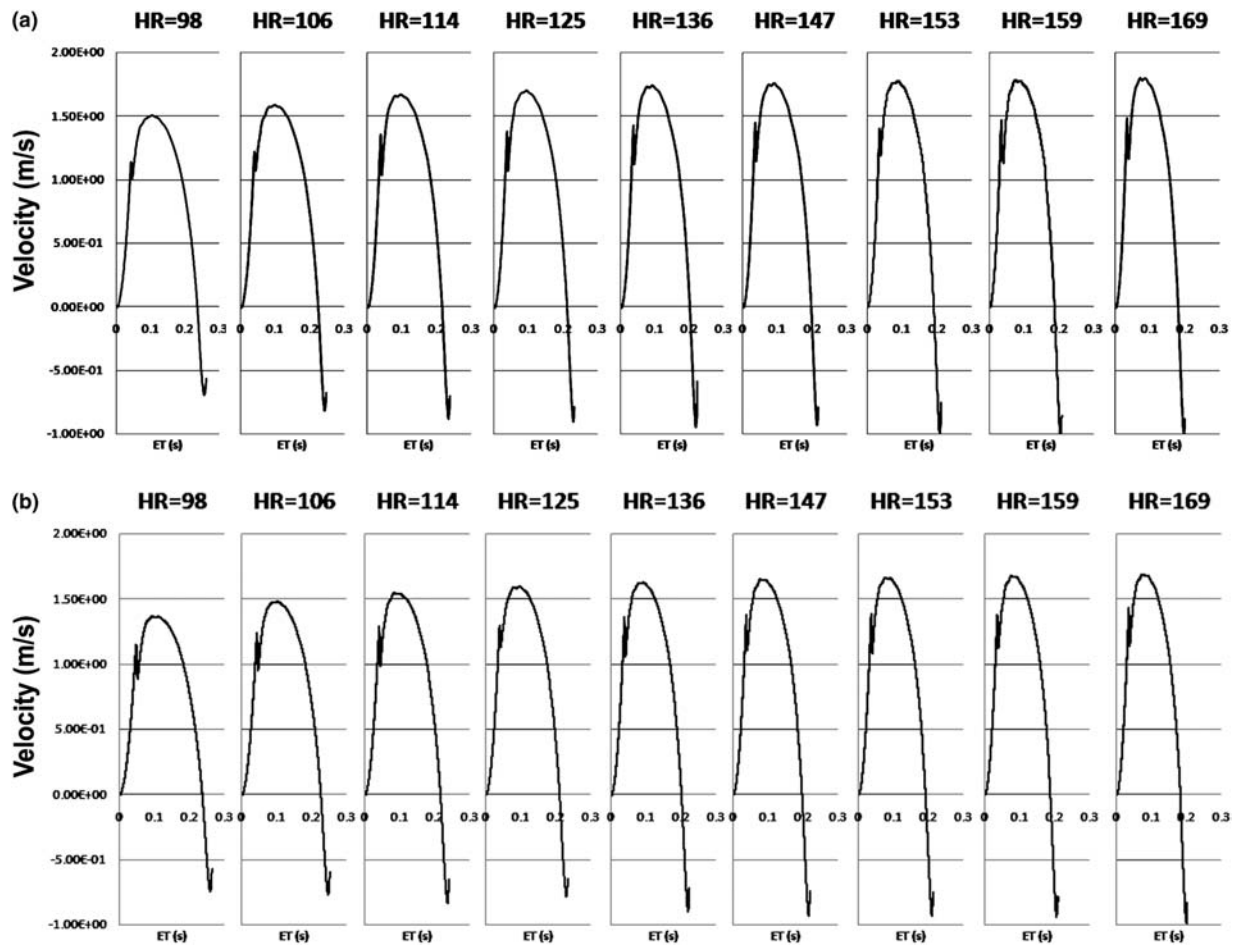


Figure 6. FSI's predictions of (a) velocity spectrums, which consider valvular-arterial pressure difference effects (stage 1). FSI's predictions of (b) velocity spectrums without valvular-arterial pressure differences effects (stage 2). Note that HR refers to heart rate and ET to ejection time.

Table 4. Comparison of echo-Doppler to numerical modelling results.

HR (bpm)	VSP/CDP (mmHg)	VSP <sup>a</sup> /CDP <sup>a</sup> (mmHg)	VPD (m/s)	VPN (m/s)	VPN <sup>a</sup> (m/s)	VMD (m/s)	VMN (m/s)	VMN <sup>a</sup> (m/s)	COD (ml/min)	CON (ml/min)	CON <sup>a</sup> (ml/min)
98	152/68	144/74	1.49	1.51	1.36	1.05	0.89	0.79	11356	9884	8773
106	158/65	152/71	1.50	1.59	1.48	1.10	0.95	0.86	12651	10864	9935
114	165/63	157/69	1.58	1.67	1.54	1.11	1.00	0.90	14051	11829	10672
125	169/63	163/69	1.60	1.70	1.59	1.21	1.03	0.94	15298	12884	11938
136	174/64	167/70	1.79	1.74	1.62	1.24	1.03	0.95	16172	13518	12489
147	178/65	171/71	1.58	1.76	1.65	1.25	1.05	0.97	17225	14600	13424
153	180/66	173/72	1.74	1.77	1.66	1.24	1.03	0.97	17330	14625	13655
159	182/67	175/72	1.77	1.78	1.68	1.26	1.06	0.97	17941	15108	13961
169	186/68	178/74	1.63	1.80	1.68	1.28	1.08	0.98	18849	15832	14504

Notes: HR, heart rate; VSP, ventricular systolic pressure; CDP, central diastolic pressure; CON, cardiac output by numerical simulation; COD, cardiac output by Doppler; SVN, stroke volume by numerical simulation, per beat; SVD, stroke volume by Doppler, per beat; VPD, peak velocity by Doppler; VPN, peak velocity by numerical simulation; VMD, mean velocity by Doppler; VMN, mean velocity by numerical simulation.

<sup>a</sup>Calculated without considering the effects of valvular–arterial pressure differences.

### 2.3.7 Calculation of cardiac output and validation

Cardiac output was computed using Equation (6):

$$\text{Cardiac output} = \text{Stroke volume} \times \text{Heart rate}, \quad (6)$$

where the stroke volume was calculated from ECG using Equation (7):

$$\text{Stroke volume} = \text{Velocity integration} \times \text{Aortic area}, \quad (7)$$

where the velocity integration was automatically obtained by tracing the Doppler flow from ultrasound imaging. The aortic area was calculated using Equation (8):

$$\text{Area} = \pi \left( \frac{D}{2} \right)^2, \quad (8)$$

where  $D$  is the measured ascending aortic diameter after the sinotubular junction (Table 1).

For FSI simulations, the mean velocity numerically was obtained at each time step of the ejection period as shown in Figures 6(a) and (b). Equation (9), however, was used to determine the velocity integration (used to determine both stroke volume and cardiac output).

$$\text{Velocity integration} = \int_0^{\text{Ejection time}} V \cdot dt, \quad (9)$$

where  $V$  is the fluid velocity through the outlet boundary. Stroke volume and cardiac output predicted from FSI simulations were compared to the values determined by echo-Doppler. Note that the mean velocity for each heart rate was obtained using Equation (10).

$$\text{Velocity mean} = \frac{\text{Velocity integration}}{\text{Ejection time}}. \quad (10)$$

Comparison of measurements of mean velocity, cardiac output and stroke volume enabled quantitative validation of the FSI model.

## 3. Results

### 3.1 Comparison of numerical and clinical haemodynamic predictions

The velocity–ejection time graphs are shown in Figures 6(a),(b) for different heart rates at rest and during exercise. Tables 4 and 5 present the data predicted from FSI simulations and echo-Doppler. The peak blood flow velocity through aorta increased by 16.6% from 98 to 147 bpm and increased a further 2.3% as the heart rate increased to 169 bpm. Figure 6(b) shows results that exclude differences between the brachial, central and aortic root pressures at the left ventricle for the velocity profiles obtained from FSI simulations at rest and for the time of exercise. When only the brachial pressure was applied as the boundary condition, velocity profiles had fewer velocity peaks than when pressure differences were accounted for. When pressure differences were accounted for, model predictions were more reliable.

The mean velocity predicted by FSI simulations was on average 14.8% lower than echo-Doppler measurements (i.e. an average for the whole protocol) when pressure differences were accounted for. This difference increased to 22.4% when the pressure differences were not accounted for (Table 4). The cardiac output predicted by FSI simulation was on average 15.4% lower when compared to echo-Doppler results, for the whole of the protocol, when pressure differences were accounted for. The corresponding difference, when pressure differences were excluded, was 22.3%.

FSI simulations that accounted for pressure differences predicted a stroke volume that was on average 15.3% lower than that derived from echo-Doppler. This increased to 26.2% when pressure differences were ignored.

For FSI simulations, the mean velocity increased by 15.7% as the heart rate increased from 98 to 136 bpm when pressure differences were accounted for and increased by 4.6% from a heart rate of 136 to 169 bpm. When pressure differences were accounted for, FSI



Table 5. Comparison of echo-Doppler to numerical modelling results in terms of stroke volume for both stages considering the effects of valvular–arterial pressure differences and not considering them.

Heart rate (bpm)	SVD (ml/beat)	SVN (ml/beat)	SVN <sup>a</sup> (ml/beat)	Sugawara et al. (2003) (ml/beat)	Christie et al. (1987) (ml/beat)	Percentage of difference of SVN to SVD
98	115.8	100.9	89.5	80	102.4	12.9
106	119.4	102.5	93.7	83	108	14.1
114	123.3	103.8	93.6	86	109.5	15.8
125	122.4	103.1	95.5	89	105	15.8
136	118.9	99.4	91.8	92	100.6	16.4
147	117.2	99.3	91.3	94	100.5	15.2
153	113.3	95.6	89.2	Na	102.5	15.6
159	112.8	95	87.8	Na	103.6	15.8
169	111.5	93.7	85.8	Na	104.7	16

Note: SVN, stroke volume by numerical simulation, per beat; SVD, stroke volume by Doppler, per beat.

<sup>a</sup> Calculated without considering the effects of valvular–arterial pressure differences.

simulations showed a 2.9% increase in stroke volume from a heart rate of 98–114 bpm. Then, this stopped from heart rates of approximately 136–147 bpm. In addition, there was a 5% decrease in stroke volume from a heart rate of 147–169 bpm (Figure 7(a)). The cardiac output (including pressure differences) increased by 60.2% from a heart rate of 98–169 bpm (Figure 7(b)). This led to an increment in cardiac output of 5984 ml/min. There were less differences between Doppler-derived data and numerical results of stage 1 (i.e. accounting for pressure differences) than that observed in stage 2 for cardiac output and stroke volume. Consequently, FSI simulation that included pressure differences were chosen to continue this study. These results also demonstrated the importance of including the valvular–vascular pressure drops in our study.

### 3.2 Correlation between FSI and echo-Doppler results

Regression analysis between echo-Doppler and FSI simulations led to a correlation gradient of 0.802 (Figure 8(a)) for cardiac output and 0.764 (Figure 8(b)) for stroke volume. The *Y*-axis intercepts for these correlations were 669.1 ml/min and 15.05 ml/beat for cardiac output and stroke volume, respectively. There was a high correlation between estimations from echo-Doppler and FSI simulations for cardiac output ( $r = 0.999$ ) and stroke volume ( $r = 0.940$ ). Therefore, there was a strong correlation between the two methods, and similar values were predicted.

### 3.3 Numerical prediction of blood backflow while accounting for pressure differences

Table 6 presents the backflow values during valve closure when the pressure difference between brachial and central/left ventricle was considered. At 98 bpm, the total cardiac output was computed to be 9884 ml/min. Backflow

averaged 489 ml/min. This led to the estimation of 4.6% backflow at the closure phase on average.

The FSI simulations predicted an increase in backflow with increased heart rate; this increased per minute by 74% from a heart rate of 98–169 bpm. The backflow increased to 498 ml/min, and the total blood volume ejected from the left ventricle was 10,373 ml/min. Moreover, backflow velocity peak increased to 43% as the heart rate increased from 98 to 169 bpm (Table 6).

### 3.4 Comparison of numerical and clinical correlation between cardiac output and brachial pressure

The relationship between cardiac output and the brachial systolic and diastolic pressure difference is shown in Figure 9. A good correlation was determined using a quadratic polynomial equation for both echo-Doppler and FSI simulations. However, a pressure difference can be estimated between the FSI simulation and the echo-Doppler-derived curve. For instance, echo-Doppler derived cardiac output for the pressure difference of 70 mmHg resulted in 11,356 ml/min. The FSI simulation, instead, estimated a cardiac output of 11,356 ml/min at 87 mmHg. This 17-mmHg difference could be due to a valvular and arterial pressure drop. An increase in the brachial pressure difference reduces this pressure drop (Figure 9).

## 4. Discussion

### 4.1 Study findings

The study has combined haemodynamic measurements with an FSI model to non-invasively calculate the cardiac output and stroke volume from a healthy subject during exercise. Echo-Doppler-derived data have been compared to FSI predictions. To our knowledge, this is the first time that an FSI model has been combined with exercise measurements to enable numerical predictions of cardiovascular performance. When valvular–vascular pressure

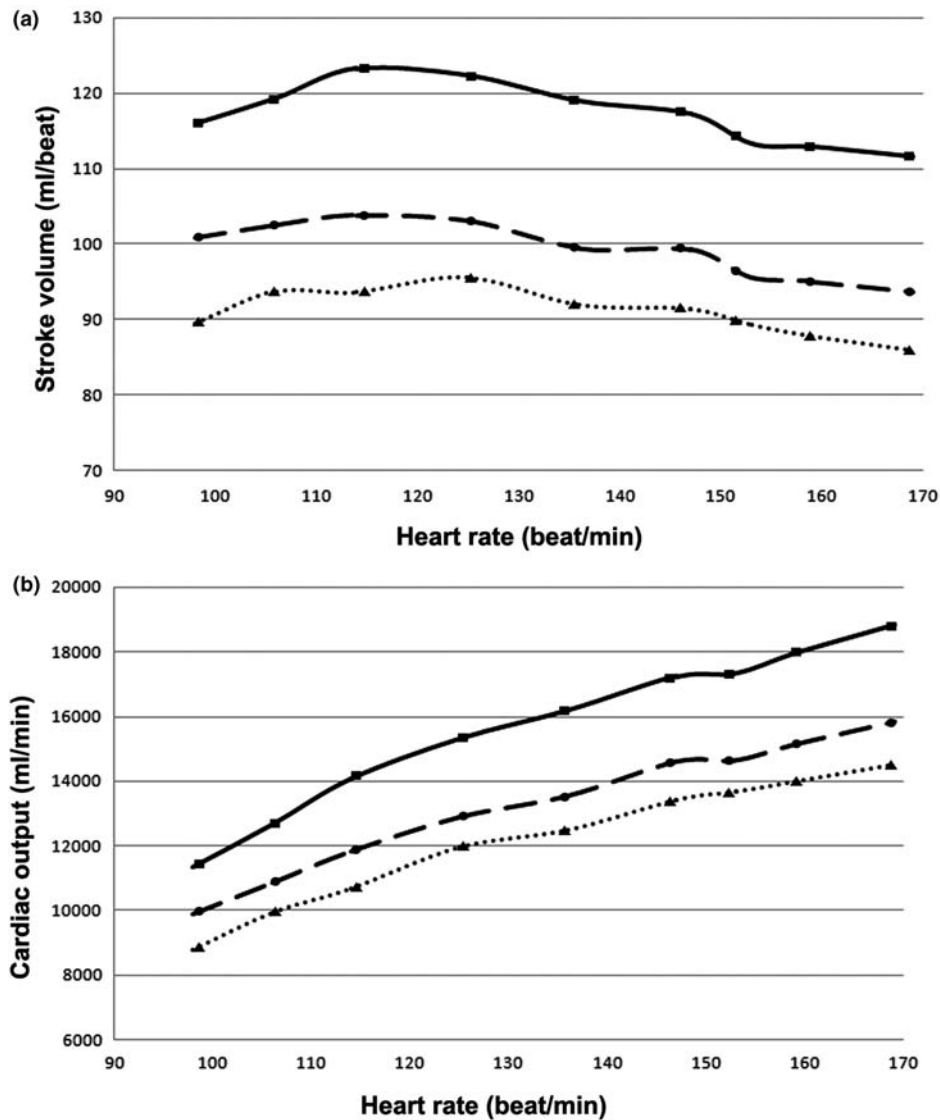


Figure 7. Comparison of (a) stroke volume and (b) cardiac output when valvular–arterial pressure differences were (broken line) and were not included (dotted line), and the Doppler-derived measurements (solid line).

differences were accounted for (stage 1), the predicted cardiac output (using FSI) was lower on average by 2415 ml/min than Doppler-derived as opposed to 3502 ml/min when such pressure differences were not accounted for (stage 2). Improved precision of the measured valvular and arterial pressure differences could further reduce the difference between the two methods. Despite the use of a simplified 2D model, FSI predicted values were within 84.6% of the Doppler-measured values. The FSI model reliably predicted the cardiac output and the mean aortic velocity over a range of heart rates. Predictions of approximately 85% of experimental measurement would present limitations in clinical use; therefore, linear correlations have been used. This enables highly accurate predictions derived from the FSI model to

be obtained (e.g.  $r = 0.94$  and  $0.999$  for stroke volume and cardiac output, respectively). This study demonstrates the feasibility of obtaining a range of time-dependent and variable boundary conditions (e.g. altered due to exercise) and generate a simplified 2D model that can predict cardiovascular performance within a relatively short solution time ( $< 20$  min).

#### 4.2 Clinical application and reliability

Catheterisation thermodilution is the gold standard for measuring the cardiac output (Lavdaniti 2008). However, it is an invasive method with potential risks such as heart failure, cardiac arrhythmia and even death (Lavdaniti 2008). In addition, thermodilution exposes the patient and

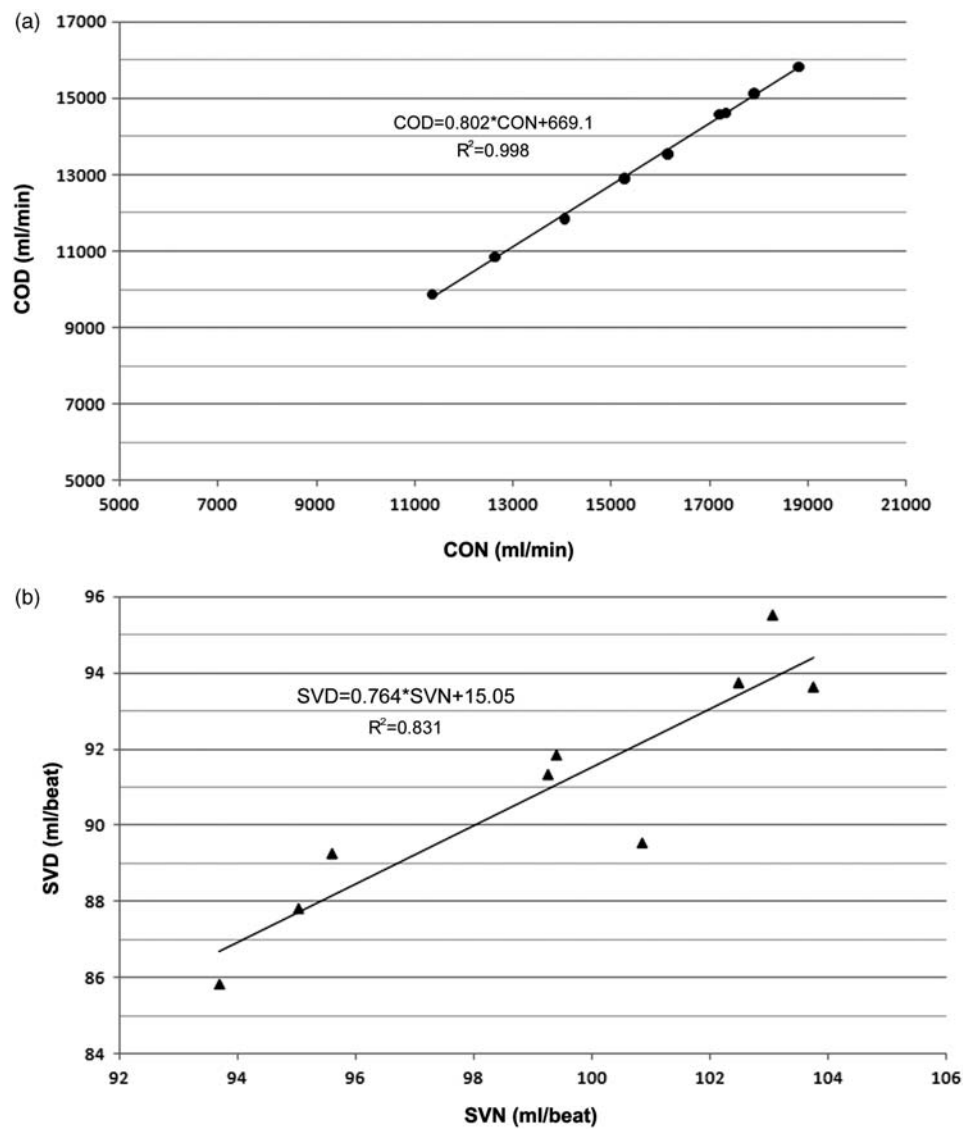


Figure 8. Regression plot (a) comparing Doppler-derived cardiac output (COD) and numerical simulation (CON). (b) Regression plot comparing Doppler-derived stroke volume (SVD) and numerical simulation (SVN).

physician to harmful radiation. Exercising while catheterized also causes a range of technical problems, and thus is not common practice. However, the application of a numerical method allows the prediction of cardiac function using non-invasive measurements throughout an exercise protocol.

Numerical simulation allows easier and more precise estimation of cardiac output than using echo-Doppler. Moreover, it does not have inter- and intra-observer validity variables that are the case when using ECG. Such variability depends on personal proficiency and the image capture capability of the user. Therefore, the key concern is the reliability of numerical methods when predicting the cardiac output.

Our FSI model led to a good cardiac output correlation with Doppler-derived values ( $r = 0.999$ ); in addition, a

Table 6. Numerical simulation estimates of backflow during closing phase.

Heart rate (bpm)	VPB (m/s)	SVB (ml/beat)	COB (ml/min)
98	− 0.70	− 5.00	− 489
106	− 0.82	− 5.32	− 563
114	− 0.88	− 5.38	− 613
125	− 0.90	− 5.11	− 637
136	− 0.95	− 5.45	− 740
147	− 0.94	− 5.28	− 776
153	− 1.01	− 5.88	− 899
159	− 1.01	− 5.34	− 849
169	− 1.00	− 5.05	− 853

Note: COB, stroke volume of backflow to left ventricular per minute; SVB, stroke volume of backflow to left ventricular per beat; VPB, backflow velocity peak.

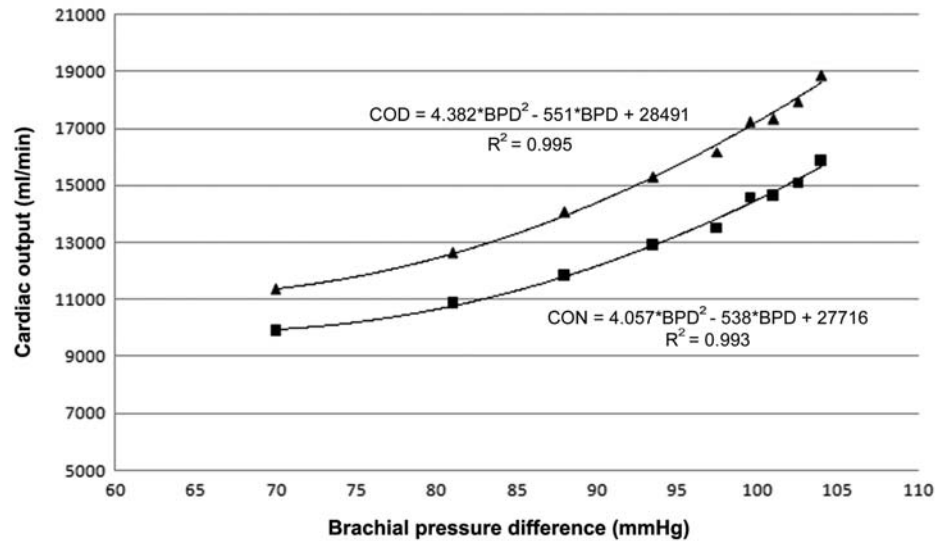


Figure 9. Regression plot (solid lines) comparing cardiac output data given by echo-Doppler (triangular points) versus numerical method (square points) related to brachial systolic and diastolic pressure difference. CON, cardiac output by numerical simulation; COD, cardiac output by Doppler; BPD, brachial pressure difference.

good correlation ( $r = 0.94$ ) was achieved for stroke volume. Data gained when accounting for pressure differences between brachial and central to aortic root at the left ventricle led to differences of 17.9 ml/beat for stroke volume on average. This increased to 26.2 ml/beat when such pressure differences were ignored. There was also a good correlation with the mean velocity ( $r = 0.94$ ), but the correlation for predicted peak velocity was lower ( $r = 0.73$ ). However, in the latter case, errors related to Doppler flow tracings may have lowered this correlation. For example, oscillations were observed at the echo-Doppler flow tip, which may have reduced the operator's tracing precision.

#### 4.3 Comparison to literature

Following a literature search, we have not found a previous comparable study that combined a clinical and numerical approach to predict cardiac function during exercise. In our study, the patient-specific cardiac output was predicted at a range of heart rates induced by exercise. However, our study compares well to other numerical studies used to predict the cardiac output at rest. Our model predicted a cardiac output at rest of 9017 ml/min, comparable to predictions between 3400 and 7500 ml/min (Korakianitis and Shi 2006; Kim et al. 2009). Such predictions have used a finite element method with a lumped parameter technique, a Wind-Kassel model (Korakianitis and Shi 2006) and an electrical integration circuit (Podnar et al. 2002). However, Podnar et al. (2002) predicted no increase in cardiac output with increased heart rate (5500 ml/min at 120 bpm, but 5300 ml/min at 150 bpm). This is in disagreement with our results because

we found cardiac output to increase with heart rate. Data derived from Christie et al. (1987) agree with our results. Therefore, it is likely that the lack of validation with clinical data, by Podnar et al. (2002), led to some inaccuracies at increased heart rates. Moreover, it should be noted that a non-athlete can be expected to have a maximum stroke volume of 110 ml with a heart rate of 195 bpm (Guyton and Hall 1996; Porth and Glenn 2010). Because our subject is a non-athlete, our numerical results are in good agreement with the literature.

#### 4.4 Limitations and future trends

This model has been used to make patient-specific predictions for cardiac output in combination with non-invasive brachial pressure measurements. A notable simplification used for our FSI model was the use of a constant orifice area and a single diameter for the ascending aorta. The regression analysis between predicted and measured cardiac output and stroke volume enables true values to be calculated from predicted model values (using the equations provided in Figure 8). Therefore, even though the model may predict a value that is approximately 15% in 'error', the true clinical value can still be derived using our existing simplified model. Validation showed good agreement with a range of haemodynamic parameters although with differences between experimental and numerical predictions. For clinical applications, further accuracy may be necessary, which may be improved by addressing key limitations.

One limitation is that the model was solved in two dimensions and, the predictions might improve by the use of a 3D model. The feasibility of developing such models



is well established (De Hart et al. 2003a, 2003b). However, a 2D model has the advantage of a shorter solution time, and this assumption has been made before for 2D valves (e.g. De Hart et al. 2000). Our model solved within 15 min which, clinically, would be a reasonable waiting time. It should be noted that existing clinical equipment have large associated errors. For example, the commercially available ultrasonograph (Maylab, 60, BIOSOUND ESAOTE Inc., CA, USA), which was used for our study and is used clinically, has a reported accuracy of  $\pm 11\%$  for the stroke volume and subsequently for the cardiac output (Maylab advanced operation, 2008).

Another limitation is that the mechanical properties of the valve leaflets specific to the volunteer are unknown. There is a large variation in the mechanical properties of all heart valves (Clark 1973) and their components (Millard et al. 2011). Although we have used accepted values in the literature, mechanical properties for each subject are not measurable. We applied a  $\pm 30\%$  change in Young's modulus (Table 7) and found that the predicted cardiac output varied by not more than 5%. It is notable that Kortsmit (2009) reported such variation in Young's modulus for a native aortic heart valve.

The assumption of rigid aortic walls was a model limitation but enabled a faster simulation time (important clinically). This limitation may contribute to the model predictions being lower than the real values measured. However, the main aim of the study was to look at the aortic valve. Consideration of the aortic wall may enable a better model in future studies. The model was also assumed isotropic, homogeneous and linear. This may have contributed to our values under-predicting the cardiac output and the stroke volume. This assumption, though, is consistent with previous studies that have led to reasonable approximations of valve function (De Hart et al. 2000; Espino et al. 2012a, 2012b).

Finally, a plane-strain simulation ignores out-of-plane effects assuming the model to be a standard cross-section of the valve. This assumption might affect the cardiac output and stroke volume predictions. However, we used an equation to mimic out-of-plane restraint to reduce

some of these errors. In addition, models not intended for use in 3D stress states include only plane-strain terms (Weinberg and Kaazempur-Mofrad 2005). Despite these above errors, the trends were predicted quite well by the model even with a 10–15% difference in magnitude. Moreover, the simplified 2D model has the advantage of solving in 6–15 min (with the computers assembled: 8 GB RAM, Core i5, 2.2 GHz) over different heart rates, which may be important clinically. Regardless of model errors, there was a very strong correlation between predicted and measured cardiac output ( $r = 0.999$ ) and stroke volume ( $r = 0.94$ ). Therefore, it is feasible to correct for predicted values (using the derived equations in Figure 8). Such methods are well established when combining a model with experimental measurement (Christie et al. 1987; Maroni et al. 1998; Sugawara et al. 2003; Park et al. 2011).

Clinical assessment of cardiac function is gathered on the basis of statistical information and generalisation. This might be considered as another limitation of our model as only one subject was investigated. However, a numerical simulation needs specific values such as boundary conditions, mechanical properties and geometric dimensions. A range of values, for statistical comparison, cannot be predicted unless stochastic modelling is applied to account for variability (Espino et al. 2003). Instead, subject-specific predictions from our FSI model were validated against directly comparable measurements. This has enabled a quantitative assessment of the reliability of our model. Currently, there is a trend towards patient-specific models in medical research (e.g. Öhman et al. 2011). This is due to the potential benefits in using numerical methods to aid treatment/diagnosis for individual patients. Recently, for example, such a 3D model was generated for an ischaemic mitral valve (Wenk et al. 2010). This presents possible applications for our combined numerical and clinical approach to investigate the cardiac output during disease, including aortic valve stenosis or even calcification, e.g. by multi-scale modelling (Weinberg and Kaazempur-Mofrad 2008).

Table 7. Change in predicted cardiac output with Young's modulus.

Young's modulus increase (%)	Change in cardiac output (%) with heart rate								
	98 (bpm)	106 (bpm)	114 (bpm)	125 (bpm)	136 (bpm)	147 (bpm)	153 (bpm)	159 (bpm)	169 (bpm)
–30	2.2	–1.1	–0.2	–4.1	–0.5	–0.4	–3.9	–3.3	–3
–20	2.3	–2.1	–1	–3.6	–0.5	–0.1	–3.4	–2.7	–3.8
–10	–0.6	–2	–0.1	–3.1	–0.2	–0.4	2.7	–2.5	–0.8
10	–0.2	–1.1	–0.1	–1.4	0.2	–0.5	0.1	0.8	–0.3
20	–2.3	–1.4	–0.1	–2.7	0.2	–0.2	–1.7	–1.9	–0.01
30	–2.7	–0.6	0.6	–2.1	1.2	–0.2	–2.2	–2.2	–0.6

## 5. Conclusion

We have introduced a 2D fluid–structure interaction model of an aortic valve, which was able to reliably predict the cardiac output and the stroke volume. Our model predicted mean velocity, stroke volume and cardiac output to within 14.8%, 15% and 15%, respectively, of echo-Doppler measurements. Strong correlations were determined for predicted and measured cardiac output ( $r = 0.999$ ) and stroke volume ( $r = 0.94$ ), which enabled correction of the numerical values predicted using regression equations. The advantage of using a simple 2D model was the relatively quick solution time of less than 15 min (important within a clinical setting). The model developed was used to make predictions both during rest and exercise.

## Acknowledgement

DME is currently supported by a Marie Curie Intra-European Fellowship within the 7th European Community Framework Programme (Programme number: FP7/2007-2013; under grant agreement n°252278).

## References

- Al-Atabi M, Espino DM, Hukins DWL. 2010. Computer and experimental modelling of blood flow through the mitral valve of the heart. *J Biomech Sci Eng.* 5(1):78–84.
- Bellhouse BJ. 1972. The fluid mechanics of heart valves. In: Bergel DH, editor. *Cardiovascular fluid dynamics*. Vol. 1. London: Academic Press. p. 261–285.
- Caro CG, Pedley TJ, Schroter RC, Seed WA. 1978. *The mechanics of the circulation*. 2nd ed. Oxford: Oxford University Press.
- Christie J, Sheldahl LM, Tristani FE, Sagar KB, Ptacin MJ, Wann S. 1987. Determination of stroke volume and cardiac output during exercise: comparison of two-dimensional and Doppler echocardiography, Fick oximetry, and thermodilution. *Circulation.* 76(3):539–547.
- Clark RE. 1973. Stress–strain characteristics of fresh and frozen human aortic and mitral leaflets and chordae tendineae. *J Thorac Cardiovasc Surg.* 66(2):202–208.
- Clark RE, Finke EH. 1974. Scanning and light microscopy of human aortic leaflets in stressed and relaxed states. *J Thorac Cardiovasc Surg.* 67(5):792–804.
- Comsol Users Manual. 2011. Comsol Multiphysics Users Guide. London: Comsol Ltd.
- Criner GJ, Barnette RE, Alonzo GE. 2010. *Critical care study guide: text and review*. 2nd ed. New York: Springer.
- De Hart J, Peters GW, Schreurs PJ, Baaijens FP. 2000. A two-dimensional fluid–structure interaction model of the aortic valve. *J Biomech.* 33(9):1079–1088.
- De Hart J, Peters GW, Schreurs PJ, Baaijens FP. 2003a. A three-dimensional computational analysis of fluid–structure interaction in the aortic valve. *J Biomech.* 36(1):103–112.
- De Hart J, Baaijens FP, Peters GW, Schreurs PJ. 2003b. A computational fluid–structure interaction analysis of a fiber-reinforced stentless aortic valve. *J Biomech.* 36(5):699–712.
- Donea J, Giuliani S, Halleux JP. 1982. An arbitrary Lagrangian–Eulerian finite element method for transient dynamic fluid–structure interactions. *Comput Methods Appl Mech Eng.* 33(1–3):689–723.
- Dowell EH, Hall KC. 2001. Modelling of fluid–structure interaction. *Annu Rev Fluid Mech.* 33(1):445–490.
- Engoren M, Barbee D. 2005. Comparison of cardiac output determined by bioimpedance, thermodilution, and the Fick method. *Am J Crit Care.* 14(1):40–45.
- Espino DM, Meakin JR, Hukins DWL, Reid JE. 2003. Stochastic finite element analysis of biological systems: comparison of a simple intervertebral disc model with experimental results. *Comput Methods Biomech Biomed Eng.* 6(4):243–248.
- Espino DM, Shepherd DET, Hukins DWL. 2012a. Evaluation of a transient, simultaneous, Arbitrary Lagrange Euler based multi-physics method for simulating the mitral heart valve. *Comput Methods Biomech Biomed Eng.*, doi: 10.1080/10255842.2012.688818.
- Espino DM, Shepherd DET, Hukins DWL. 2012b. Transient large strain contact modelling: a comparison of contact technique for simultaneous fluid–structure interaction. *Comput Fluids.*
- Espino DM, Shepherd DET, Hukins DWL. 2012c. Development of a transient large strain contact method for biological heart valve simulations. *Comput Methods Biomech Biomed Eng.* doi: 10.1080/10255842.2011.623676.
- Formaggia L, Nobile F. 1999. A stability analysis for the arbitrary Lagrangian Eulerian formulation with finite elements. *East-West J Numer Math.* 7(2):105–132.
- Govindarajan V, Udaykumar HS, Herbertson LH, Deutsch S, Manning KB, Chandran KB. 2010. Two-dimensional FSI simulation of closing dynamics of a tilting disk mechanical heart valve. *J Med Dev.* 4(1), 011001(1–11).
- Guyton AC, Hall JE. 1996. *Textbook of medical physiology*. 9th ed. Philadelphia, PA: WB Saunders.
- Hofer CK, Ganter MT, Zollinger A. 2007. What technique should I use to measure cardiac output? *Curr Opin Crit Care.* 13(3):308–317.
- Kim HJ, Vignon-Clementel IE, Figueroa CA, LaDisa JF, Jansen KE, Feinstein JA, Taylor CA. 2009. On coupling a lumped parameter heart model and a three-dimensional finite element aorta model. *Ann Biomed Eng.* 37(11):2153–2169.
- Knobloch K, Hoeltke V, Jakob E, Vogt PM, Phillips R. 2007a. Non-invasive ultrasonic cardiac output monitoring in exercise testing. *Int J Cardiol.* 126(3):445–447.
- Knobloch K, Spies M, Vogt PM, Phillips R. 2007b. A comparison of real-time CW Doppler and calculated cardiac output according to the Stringer formula for non-invasive hemodynamics in exercise testing. *Int J Cardiol.* 131(3):413–415.
- Koch TM, Reddy BD, Zilla P, Franz T. 2010. Aortic valve leaflet mechanical properties facilitate diastolic valve function. *Comput Methods Biomech Biomed Eng.* 13(2):225–234.
- Korakianitis T, Shi Y. 2006. Numerical simulation of cardiovascular dynamics with healthy and diseased heart. *J Biomech.* 39(11):1964–1982.
- Kortsmit J. 2009. Non-invasive assessment of leaflet deformation and mechanical properties in heart valve tissue engineering [dissertation]. [Eindhoven]: Technische Universiteit Eindhoven.
- Laske A, Jenni R, Maloigne M, Vassalli G, Bertel O, Turina MI. 1996. Pressure gradients across bileaflet aortic valves by direct measurement and echocardiography. *Ann Thorac Surg.* 61(1):48–57.
- Lavdaniti M. 2008. Invasive and non-invasive methods for cardiac output measurement. *Int J Caring Sci.* 1(3):112–117.
- Maylab Users Manual. 2008. Maylab advanced operation. New York: BIOSOUND ESAOTE Inc.

- Maroni JM, Oelberg DA, Pappagianopoulos P, Boucher CA, Systrom DM. 1998. Maximum cardiac output during incremental exercise by first-pass radionuclide ventriculography. *Chest*. 114(2):457–461.
- Millard L, Espino DM, Shepherd DET, Hukins DWL, Buchan KG. 2011. Mechanical properties of chordae tendineae of the mitral heart valve: Young's modulus, structural stiffness and effects of aging. *J Mech Med Biol*. 11(1):221–230.
- Murphy SL, Xu J. 2012. Deaths: preliminary data for 2010. 1st ed. Atlanta: National Vital Statistics Reports.
- Öhman C, Espino DM, Heinmann T, Baleani M, Delingette H, Viceconti M. 2011. Subject-specific knee joint model: design of an experiment to validate a multi-body finite element model. *Visual Comput*. 27(2):153–159.
- Park SH, Lee SJ, Kim JY, Kim MJ, Lee JY, Cho AR, Lee HG, Lee SW, Shin WY, Jin DK. 2011. Direct comparison between brachial pressure obtained by oscillometric method and central pressure using invasive method. *J Soon-chunhyang Med Sci*. 17(2):65–71.
- Peskin CS. 1972. Flow patterns around heart valves: a numerical method. *J Comput Phys*. 10(2):252–270.
- Peskin CS. 1977. Numerical analysis of blood flow in the heart. *J Comput Phys*. 25(3):220–252.
- Podnar T, Runovc F, Kordas M. 2002. Simulation of cardiovascular physiology: the diastolic function(s) of the heart. *Comput Biol Med*. 32(5):363–377.
- Porth CM, Glenn G. 2010. Pathophysiology: concepts of altered health states. 7th ed. Philadelphia: Lippincott Williams & Wilkins.
- Smith FG, Yeung J. 2010. Core topics in critical care medicine. book auth. 1st ed. New York: Cambridge University Press.
- Stijnen JMA, De Hart J, Bovendeerd PHM, Van de Vosse FN. 2004. Evaluation of a fictitious domain method for predicting dynamic response of mechanical heart valves. *J Fluids Struct*. 19(6):835–850.
- Stouffer GA. 2008. Aortic regurgitation. Cardiovascular hemodynamics for the clinician. Oxford: Wiley–Blackwell.
- Stringer WW, Hansen JE, Wasserman K. 1997. Cardiac output estimated noninvasively from oxygen uptake during exercise. *J Appl Physiol*. 82(1):908–912.
- Sugawara J, Tanabe T, Miyachi M, Yamamoto K, Takahashi K, Iemitsu M, Otsuki T, Homma S, Maeda S, Ajisaka R, et al., 2003. Non-invasive assessment of cardiac output during exercise in healthy young humans: comparison between Modellflow method and Doppler echocardiography method. *Acta Physiol Scand*. 179(4):361–366.
- Van de Vosse FN, De Hart J, Van Oijen CHGA, Bessems D, Gunther TWM, Segal A, Wolters BJBM, Stijnen JMA, Baaijens FPT. 2003. Finite-element-based computational methods for cardiovascular fluid–structure interaction. *J Eng Math*. 47(3–4):335–368.
- Wall W, Gerstenberger A, Gamnitzer P, Forster C, Ramm E. 2006. Large deformation fluid–structure interaction – advances in ALE methods and new fixed grid approaches. In: Bungartz HJ, Shafer M, editors. Fluid–structure interaction. Berlin: Springer. p. 195–232.
- Weinberg EJ, Kaazempur-Mofrad MR. 2008. A multiscale computational comparison of the bicuspid and tricuspid aortic valves in relation to calcific aortic stenosis. *J Biomech*. 41(16):3482–3487.
- Weinberg EJ, Kaazempur-Mofrad MR. 2005. On the constitutive models for heart valve leaflet mechanics. *Cardiovasc Eng*. 5(1):37–43.
- Wenk JF, Zhang Z, Cheng G, Malhotra D, Acevedo-Bolton G, Burger M, Suzuki T, Saloner DA, Wallace AW, Guccione JM, et al., 2010. The first finite element model of the left ventricle with mitral valve: insights into ischemic mitral regurgitation. *Ann Thorac Surg*. 89(5):1546–1553.
- Winslow AM. 1966. Numerical solution of the quasilinear poisson equation in a nonuniform triangle mesh. *J Comput Phys*. 1(2):149–172.
- Xia GH, Zhao Y, Yeo JH. 2005. Numerical Simulation of 3D fluid–structure interaction using AN immersed membrane method. *Mod Phys Lett B*. 19(28–29):1447–1450.